Nuclear Instruments and Methods in Physics Research B 571 (2026) 165960

Contents lists available at ScienceDirect

Nuclear Inst. and Methods in Physics Research, B

journal homepage: www.elsevier.com/locate/nimb

Full length article

Measurement and compensation of electric field disturbances of an electrostatic deflector☆

Markus Schiffer *, Ferhat Altun, Dennis Mücher

Institute for Nuclear Physics, University of Cologne, Germany

ARTICLE INFO

Keywords:
AMS
Ion cooler
Electrostatic deflector
Field measurement
Field compensation

ABSTRACT

For the decoupling of a high intense laser beam from an ion beam, the outer electrode of an electrostatic deflector was built with a hole, behind that an additional correction electrode was installed to correct for field disturbances. This electrostatic deflector is installed at the Anion Laser Isobar Separator - ALIS, at the 6 MV Accelerator Mass Spectrometry (AMS) system of the University of Cologne. A novel technique for the measurement of electric field strength and electric field disturbances was developed to show the functionality of the correction electrode. An RF voltage was applied to the electrodes of the electrostatic deflector and the induced power to a capacitive probe was measured by use of a simple spectrum analyzer. With this approach it is possible to measure electric field strength over 3 orders of magnitude, between 0.148 V/m and 149 V/m, with a resolution of 2.8%.

1. Introduction

The Anion Laser Isobar Separator (ALIS) is an extension to the 6 MV Accelerator Mass Spectrometry system at the University of Cologne [1]. Its purpose is to suppress anion isobars by element-selective laser-photodetachment in a radiofrequency quadrupole (RFQ) ion cooler [2]. This mechanism relies on the neutralization of the weakly bound additional electron of the unwanted isobaric anion by the laser. For this purpose, the laser energy is chosen to be greater than the electron affinity of the isobaric anion electron affinity but less than the electron affinity of the desired anion [3]. In order to realize the decoupling of the high intense laser beam from the ion beam, the outer electrode of the electrostatic deflector was built with a hole, similar to the setup described in [4]. This decoupling hole within the electrostatic deflector will cause electrostatic field disturbances and they are expected to increase the background due to unwanted ion paths. For this reason, the aim of this work is to detect deviations in the electric field and to prove the possibility of correcting this deviation by means of an additional field correcting electrode behind the decoupling hole.

2. Electrostatic deflector

The 90° electrostatic deflector (ESD) is used for the energy filtering of the anion beam. For the use of the ALIS setup at the CologneAMS 6 MV facility, the ESD comes with the necessity of including a decoupling hole for the laser beam as can be seen in Fig. 1. Consequently, a disturbance in the electric field of the ESD is expected to occur near to the decoupling hole. The decoupling hole should be as small as possible to minimize the disturbance, but the laser beam has to pass the decoupling hole and this will restrict the maximal divergence of the laser beam. In this particular case, a hole diameter of 6 mm restricts the laser beam to a divergence of 0.82 mrad.

Different hole sizes were simulated with SIMION 8.1 ((Scientific Instrument Services by Adaptas, Palmer, MA, USA)) for the quantification of the field disturbance and the results for 3 mm, 4 mm, 5 mm, 6 mm are compared to the undisturbed field in Fig. 2. The electric field strength was determined along a radial path that passes trough the decoupling hole. An inclination of this path to the laser axis of 71.4° was chosen, as well as a grid cell size of 0.5 mm. As a result, the field disturbance increases to up to 44% at a radial position of 315 mm, marking the position where the outer electrode should start. It has to be pointed out, that this difference is independent of the hole size. The radial disturbance is more shallow for smaller hole diameter. Smaller hole diameter will of course reduce the area, where the disturbance is present, since it will only appear in front of the hole. Close to the surface of the electrode the data show partially a non-smooth behavior of the field strength, that is originated in the approximation of the electrode by the grid cell size, and the results are not accurate close to the model surface. This represents a general limitation of electric field simulations.

☆ This article is part of a Special issue entitled: 'Special Issue of AMS16' published in Nuclear Inst. and Methods in Physics Research, B.

* Corresponding author.
E-mail address: mschiffer@ikp.uni-koeln.de (M. Schiffer).

https://doi.org/10.1016/j.nimb.2025.165960
Received 31 May 2025; Received in revised form 17 November 2025; Accepted 25 November 2025
Available online 1 December 2025

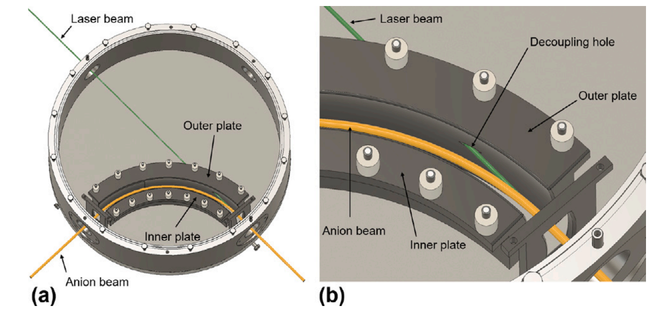

Fig. 1. (a) Inclined top view of the CAD 3D model of the ESD installed at ALIS. The ion beam is marked in orange and the laser is marked in green. (b) Detailed view of the decoupling hole.

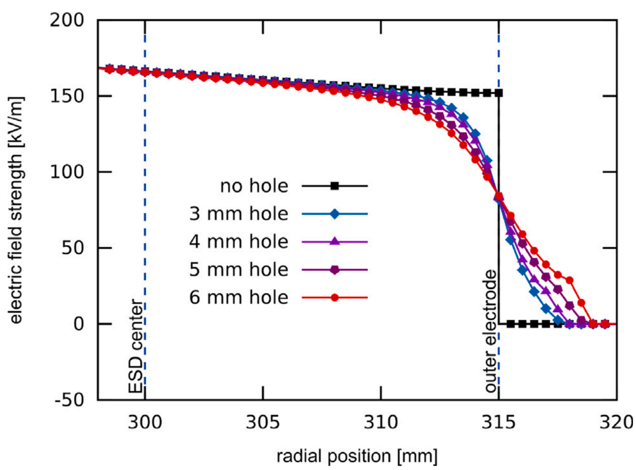

Fig. 2. Simulation of the electric field strength for different decoupling hole diameters, along a radial path through the decoupling hole. A operation voltage of ± 2.5 kV was used for the simulation. The center of the ESD, where the nominal ion path is located, as well as the outer electrode boundary is marked with a blue dashed lines.

By adding an electrode behind the decoupling hole, compensation of the electric field disturbance becomes possible. Therefore, a fanned out decoupling hole was designed, that opens to the back of the electrode, and allows the installation of a curved correction electrode. The sectional view of the laser/ion beam decoupling setup is presented in Fig. 3. It shows how the laser beam can pass the correction electrode. For the fanned out decoupling hole a 6 mm diameter was chosen, because of the restriction to the laser beam divergence.

The simulation of the equipotential lines ($\Delta U = 100$ V) for (a) 3 mm hole, (b) 6 mm hole, (c) without a correction voltage at the additional electrode behind the fanned out hole and (d) with a correction voltage are shown in Fig. 4. For the simulation a typical operation voltage of ± 2.5 kV was used, that is needed for 25 keV anions and the chosen ESD geometry. The simulation for all these cases show a strong bulge of the equipotential lines close to the outer electrode. The quantitative analysis for the electric field strength along the radial path is shown in Fig. 5. First, the fanned out decoupling hole with the correction electrode at the same voltage as the outer electrode with -2.5 kV shows nearly the same electric field strength distribution like a the 6 mm hole . When a higher voltage is used at the correction electrode the disturbance in the electric field strength can be corrected . For this particular geometry, e.g. the distance of the hole to the correction electrode, the electric field disturbance was reduced lower than 4%, with a voltage of -14 kV.

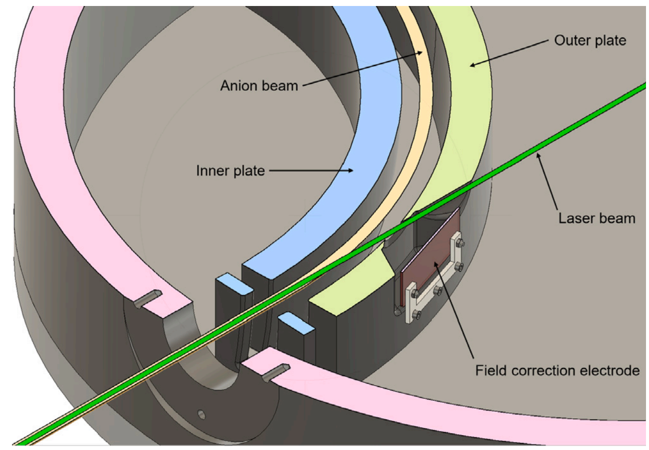

Fig. 3. Sectional view of the laser/ion beam decoupling setup.

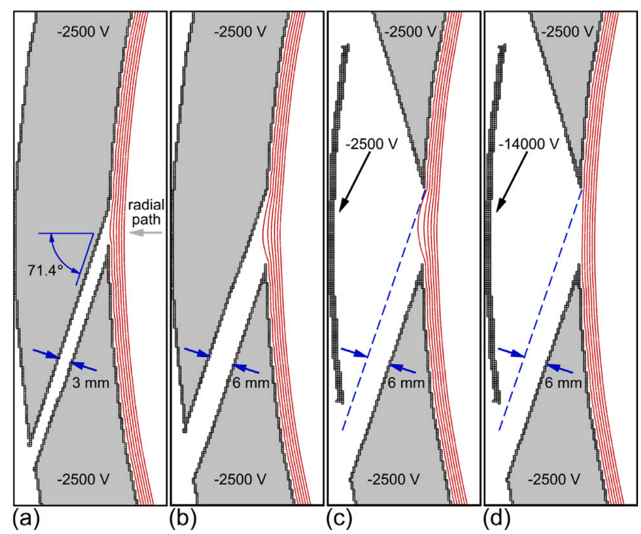

Fig. 4. Simulation of the equipotential lines ($\Delta U = 100$ V) for (a) 3 mm hole, (b) 6 mm hole, (c) without a correction voltage at the additional electrode behind the fanned out hole and (d) with a correction voltage. Calculated with a typical operation voltage of ± 2.5 kV. The bulged lines in front of the decoupling hole indicate the disturbance in the electric field.

3. Methods

In order to examine the electric field strength of the electrostatic deflector in the undisturbed area and in front of the opening in the outer plate, a new measurement technique has been developed, that can be applied in any capacitive device. First, the measuring range and resolution were determined by a measurement in a plate capacitor, then the electric field disturbance was measured using a position scan parallel to the outer electrode.

3.1. Electric field measurement method

A capacitive probe was placed inside of the capacitive device under test, that is connected to a RF signal from a function generator. The amplitude V_0 of the signal generator could be varied up to 5 V. The frequency f of the applied voltage, given by $V = V_0 \cdot sin(\omega t + \vartheta_V)$, was held constant at 25 MHz, with $\omega = 2\pi \cdot f$. Because of the capacitive coupling of the probe to the device under test, the resulting current I_0 is proportional to the capacity C between the probe and the electrode carrying the RF voltage. Certainly, the resistance R and inductance L

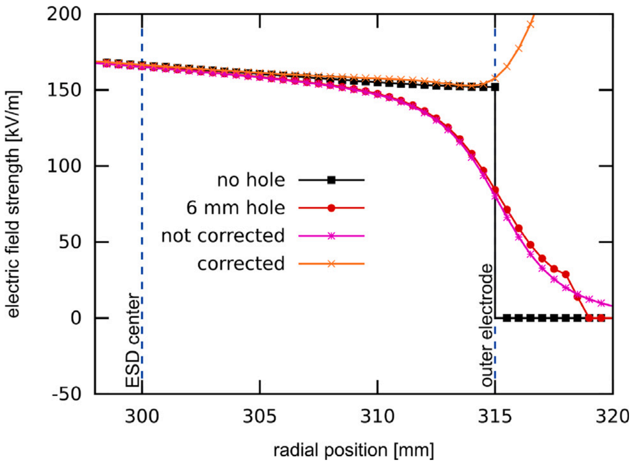

Fig. 5. Simulation of the electric field strength for different decoupling hole types along a radial path through the decoupling hole. A correction electrode voltage of −2.5 kV for the not corrected case and −14 kV for the corrected case was used in the simulations, as well as a operation voltage of ±2.5 kV. The center of the ESD, where the nominal ion path is located, as well as the outer electrode boundary is marked with blue dashed lines.

of the probe and measurement device contribute to the total impedance $Z = R + i\omega L + \frac{1}{i\omega C}$ and the phase difference $\Theta = \vartheta_V - \vartheta_I$ between the voltage and current, see schematic diagram in Fig. 6.

$$I = I_0 \cdot sin(\omega t + \vartheta_I) = \frac{V_0}{Z} \cdot sin(\omega t + \vartheta_I)$$

The capacitive coupling is dominated by the size of the active surface of the probe and the distance to the electrode carrying the RF voltage. In this particular case a commercial near-field-probe on a pcb-board was used, that is usually used in electromagnetic compatibility compliance tests [5]. These E-field probes act as wide bandwidth antenna and are simple coaxial antennas, where the central conductor protrudes out of the coaxial shield [6]. The dimensions of the active surface of the used probe are 5 mm × 0.5 mm.

A tinySA spectrum analyzer was used to measure the time-averaged power induced to the capacitive probe, which is proportional to the electric field due to the capacitive coupling.

$$\langle P \rangle = \frac{V_0}{\sqrt{2}} \cdot \frac{I_0}{\sqrt{2}} \cdot cos(\Theta) = \frac{V_0^2}{2 \cdot Z} \cdot cos(\Theta) \propto |\vec{E}[V/m]|$$

All measurement of the time-averaged power were carried out with zero span at the center frequency of 25 MHz in the resolution bandwidth of 200 Hz. The average power was measured over 200 ms, with a resolution of 0.5 dBm.

3.2. Resolution and measuring range

The proportionality between the measured RF power and the electric field strength includes the weak capacitive coupling between the device under test and the capacitive probe, as well as the input impedance of the spectrum analyzer. The calibration of the electric field strength for the applied RF voltage amplitude can be done with any capacitor, where the field is homogeneous over the volume of the capacitive probe. It has to be pointed out, that a change in capacitance will result in a difference in RF power, no matter at which field strength it is positioned in. In this particular case, a parallel plate capacitor with a diameter of 54 mm and a plate distance of d = 1.6 mm was used, without a change of the probe position or distance to the electrodes, hence without change of the capacitance.

As a result the time-averaged power was measured for applied voltages in the range of 0 to 5 V. By use of the known relationship between the voltage and electric field strength of a parallel plate capacitor, this

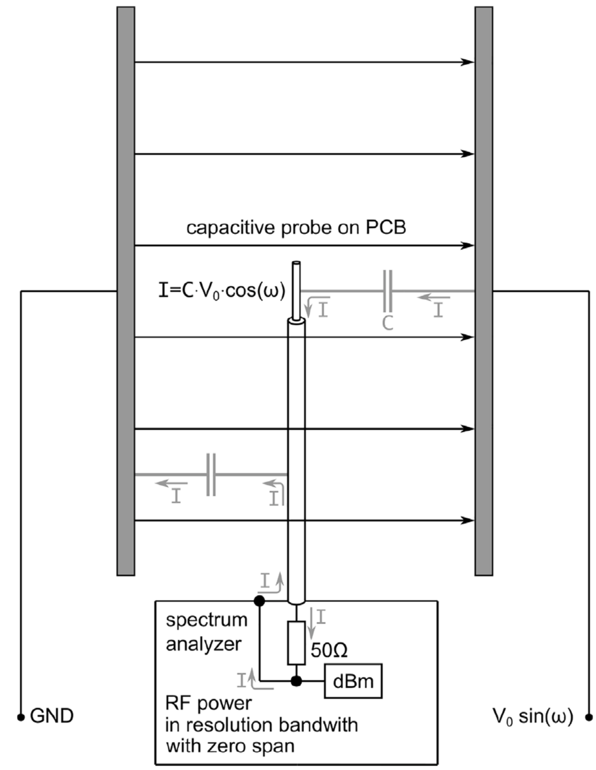

Fig. 6. Schematic circuit diagram of the electric field measurement. The capacitive device under test is connected to a RF signal from a function generator. In this example a parallel plate capacitor is shown. A tinySA spectrum analyzer was used with zero span at the center frequency of 25 MHz. Therefore, it measured the time-averaged power in the resolution bandwidth of 200 Hz.

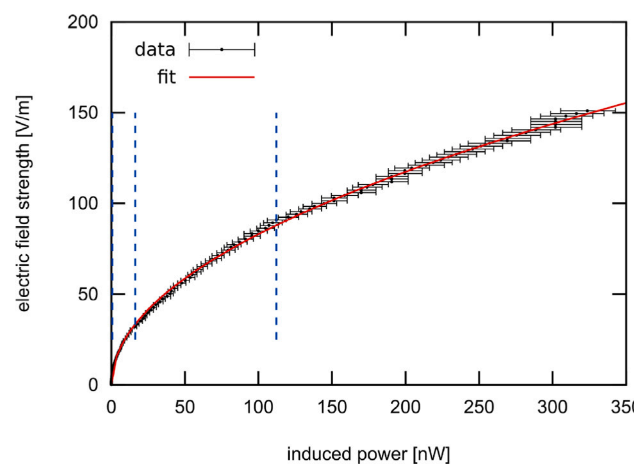

Fig. 7. Calibration curve which assigns the induced power in nW to the electric field in V/m. The measured curve has been fitted to a function of the form $|\vec{E}| = a \cdot \sqrt{P}$ using the least squares method, with $a = (8.30 \pm 0.01)$.

was assigned accordingly $|\vec{E}| = V_0/d$. The measured power in dBm can be converted to nW: $P[nW] = 10^{\frac{P[dBm]}{10}} \times 10^6$. Because the inverse function has to be used later for the calibration, a fit function of the form $|\vec{E}| = a \cdot \sqrt{P}$ was used, see Fig. 7. The vertical blue dashed lines indicates switching thresholds of the RF generators. The resulting calibration function in units of nW and V/m is:

$$|\vec{E}[V/m]| = (8.30 \pm 0.01)\sqrt{P[nW]} \quad (1)$$

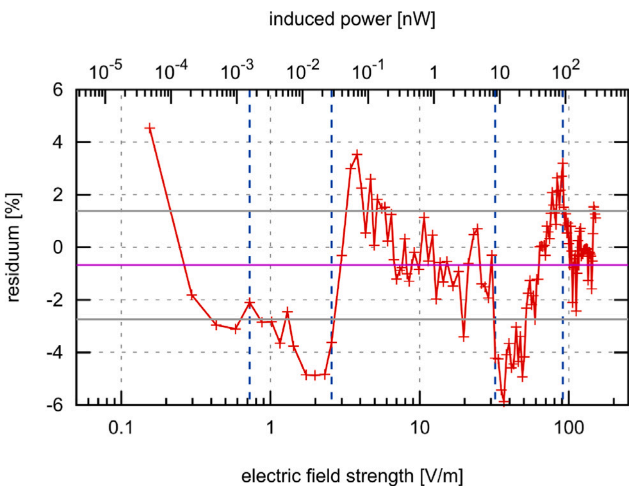

Fig. 8. Residuum plot for the calibration function (1). The vertical blue dashed lines indicating internal switching thresholds of the RF generator. Horizontal solid purple line represents the mean residuum and the gray lines the corresponding standard deviation.

For the determination of the resolution and measuring range, the residuum of the measurement is plotted in Fig. 8. All consecutive data points are connected by a line to guide the eye. The electric field strength is shown in logarithmic scale. Internal switching thresholds of the RF generator, where the output voltage ranges switch, have produced huge deviations. This was also visible in the Fourier transform of the output signal, where large changes in the higher order harmonics occurred. They are indicated by vertical blue dashed lines. Horizontal solid purple line represents the mean residuum of −0.7% and the gray lines the corresponding standard deviation of 2.1%. This demonstrates that with the new approach to measuring electric field strength, it is possible to achieve measurements spanning more than three orders of magnitude, from 0.148 V/m to 149 V/m, with a resolution of 2.8%.

3.3. Calibration for field measurement

To measure the electric field strength with the new method in an other device under test, the dissipated power has to be calibrated to the applied RF voltage V_0, while the capacity is held constant. The here used ESD has spherically shaped plates. Hence, the electric field is described by the electric field of a spherical capacitor $\vec{E}(r) = \frac{Q}{4\pi\epsilon}\frac{\vec{e}_r}{r^2}$ and the electric field strength can be calculated by $|\vec{E}(r)| = \frac{R_1 R_2}{R_2 - R_1}\frac{U}{r^2}$ from the voltage difference of the plates U and the geometry, $R_1 = 285$ mm and $R_2 = 315$ mm radii, for the fixed position r of the capacitive probe. The curved correction electrode has a radius of $R_3 = 338$ mm. It has to be noted, that the movement of the capacitive probe with fixed distance parallel to the electrode will give the same result because it will not change the capacitance.

The relationship shown in Fig. 9 allows to determine the electric field by measuring the electric power with the spectrum analyzer. Finally, the calibration function in units of nW and V/m is:

$$|\vec{E}_{ESD}[\mathrm{V/m}]| = (9.20 \pm 0.02)\sqrt{P[\mathrm{nW}]} \quad (2)$$

In contrast to the resolution measurement in Section 3.2, where the average power was measured over 200 ms, the spectrum analyzer recorded with steps of 0.5 dBm. This sort of binning is associated with an uncertainty of $\Delta L_\mathrm{P} = 0.25$ dBm.

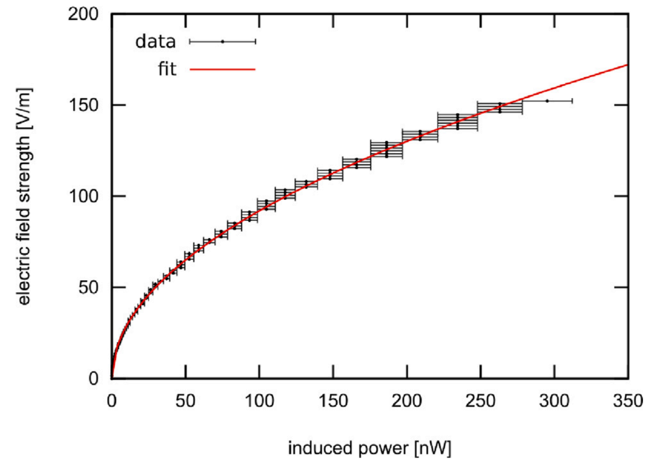

Fig. 9. Calibration curve for the ESD, which assigns the induced power in nW to the electric field in V/m, (1.55 ± 0.05) mm in front of the electrode. The measured curve has been fitted to a function of the form $|\vec{E}| = a \cdot \sqrt{P}$ using the least squares method, with $a = (9.20 \pm 0.02)$.

Table 1
Amplitude parameters for the settings of the electric field measurements.

Setting	V_{R_1} [V]	V_{R_2} [V]	V_{R_3} [V]	Color (Fig. 10)
Over-corrected	0	0.2	5	Black
Not corrected	0	0.1	0.1	Red

4. Results and discussion

4.1. Electric field measurement

The data acquisition was conducted by sliding the capacitive probe on a fixed circular trajectory parallel to the outer electrode of the ESD. For this purpose, a probe holder was 3D printed to ensure a precise positioning. The distance of the probe to the outer electrode was (1.55 ± 0.05) mm. The position was measured on the outside of the ESD, due to its spherical shape. Because of the measurement principle, the outer electrode of the ESD, as well as the field correction electrode, were connected to a two-channel function generator. Both channels were set to 25 MHz and the phase shift between both signals was compensated by the adjustment of the output phase of the function generator, Rigol DG1022. An oscilloscope was used for monitoring the phase and amplitude of both signals. The inner electrode of the ESD was connected to ground.

However, if the capacitive probe slides on a fixed circular trajectory in front of the hole in the outer plate, the capacity will change. Therefore, two measurements were compared to show the effect of the correction electrode, one over-corrected with high voltage on the correction electrode and an other where it is on the same potential as the outer plate of the ESD. The used parameters are shown in Table 1, where the colors correspond to Fig. 10. There are the geometric boundaries of start and end point of the hole are marked with a vertical purple line.

Since the capacitance between probe and correction electrode is certainly lower than the capacitance between probe and outer electrode, the increase in the measured electric field strength in front of the hole shows an over-correction of the expected dip without a field correction.

The result is in a good agreement with the simulation with SIMION 8.1, which were done for the simulated geometry of Fig. 3, with the parameters of Table 1.

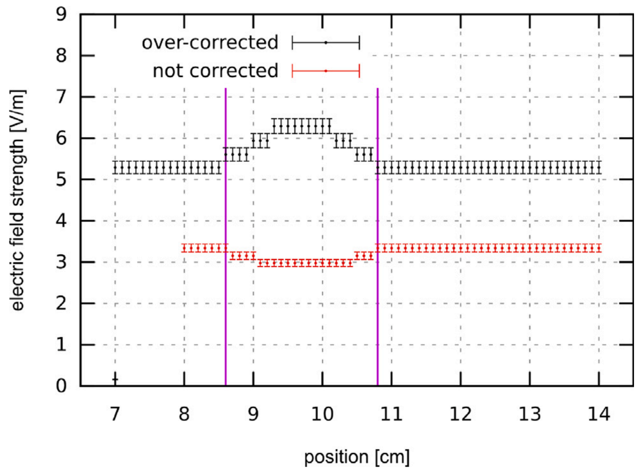

Fig. 10. Electric field within the ESD on a fixed radius as a function of its position along the curved ESD with (black) and without (red) field correction. The geometric boundary of start and end point of the hole is marked with a vertical purple line.

5. Conclusion and outlook

The decoupling hole in the outer electrode of the electrostatic deflector, through which the laser is directed to the power meter, causes a significant disturbance in the electric field. Such a disturbance may lead to an increase in the background in an AMS measurement due to the refocusing of scattered particles. By the addition of an correction electrode behind the hole, the electric field can be corrected. Simulations have indicated this potential improvement.

For the measurement of the electric field and its disturbance, a new measurement method was successfully developed in this work. This method uses a high-frequency voltage applied to the test object and the induced power is measured by use of a capacitive probe with a spectrum analyzer. With this approach it is possible to measure electric field strength over 3 orders of magnitude, between 0.148 V/m and 149 V/m, with a resolution of 2.8%. The weakness of the method is the dependence of the capacitive coupling. Nonetheless, it allows comparative measurements, that have shown the functionality of the correction electrode.

Considering further steps, once the ALIS setup is fully operational, the exact voltage for the field correcting electrode has to be determined experimentally and the change of background has to be investigated during full AMS measurements.

CRediT authorship contribution statement

Markus Schiffer: Writing – original draft, Project administration, Methodology, Investigation, Formal analysis, Conceptualization. **Ferhat Altun:** Writing – review & editing, Visualization, Investigation, Formal analysis. **Dennis Mücher:** Validation, Supervision, Funding acquisition.

Declaration of competing interest

Authors wish to confirm that there are no known conflicts of interest associated with this publication and there has been no significant financial support for this work that could have influenced its outcome.

References

[1] A. Dewald, S. Heinze, C. Feuerstein, C. Müller-Gatermann, A. Stolz, M. Schiffer, G. Zitzer, T. Dunai, J. Rethemeyer, M. Melles, H. Wiesel, F. von Blanckenburg, The first year of operation of cologneams; performance and developments, EPJ Web Conf. 63 (2013) 03006, http://dx.doi.org/10.1051/epjconf/20136303006.

[2] M. Schiffer, O. Machhart, A. Priller, S. Herb, G. Hackenberg, S. Heinze, M. Martschini, E. Strub, T. Dunai, R. Golser, A. Dewald, An advanced radio-frequency quadrupole ion cooler for accelerator mass spectrometry, Nucl. Instrum. Methods Phys. Res. Sect. B: Beam Interact. Mater. Atoms (ISSN: 0168-583X) 528 (2022) 27–33, http://dx.doi.org/10.1016/j.nimb.2022.07.010, URL https://www.sciencedirect.com/science/article/pii/S0168583X22001847.

[3] M. Martschini, J. Pitters, T. Moreau, P. Andersson, O. Forstner, D. Hanstorp, J. Lachner, Y.L., A. Priller, P. Steier, R. Golser, Selective laser photodetachment of intense atomic and molecular negative ion beams with the ILIAS RFQ ion beam cooler, Int. J. Mass Spectrom. (ISSN: 1387-3806) 415 (2017) 9–17, http://dx.doi.org/10.1016/j.ijms.2016.12.015, URL https://www.sciencedirect.com/science/article/pii/S1387380616302378.

[4] M. Martschini, D. Hanstorp, J. Lachner, C. Marek, A. Priller, P. Steier, P. Wasserburger, R. Golser, The ILIAMS project – an RFQ ion beam cooler for selective laser photodetachment at VERA, Nucl. Instrum. Methods Phys. Res. Sect. B: Beam Interact. Mater. Atoms (ISSN: 0168-583X) 456 (2019) 213–217, http://dx.doi.org/10.1016/j.nimb.2019.04.039, URL https://www.sciencedirect.com/science/article/pii/S0168583X1930223X.

[5] J. Pawson, Graphic guide to EMC – near field probing, 2021.

[6] W.G. Fano, Standard electric and magnetic field for calibration, in: Electric Field, IntechOpen, Rijeka, 2018, http://dx.doi.org/10.5772/intechopen.72687.